



Version: 1.6

**Search for the Higgs boson
in $H \rightarrow WW^* \rightarrow ll'$ ($l, l' = e, \mu$) decays with 950 pb⁻¹ at DØ in Run II**

The DØ Collaboration
URL <http://www-d0.fnal.gov>
(Dated: March 17, 2006)

A search for the Higgs boson is presented in $H \rightarrow WW^* \rightarrow ll'$ ($l, l' = e, \mu$) decays in $p\bar{p}$ collisions at a center-of-mass energy of $\sqrt{s} = 1.96$ TeV. Final states containing either two electrons e^+e^- or an electron and a muon $e^\pm\mu^\mp$ have been considered. The data, corresponding to an integrated luminosity of the order of ~ 950 pb⁻¹, have been collected from April 2002 to November 2005 with the Run II DØ detector. No significant excess above the Standard Model background has been observed and upper limits on the production cross section times branching ratio $\sigma \times BR(H \rightarrow WW^*)$ are presented on the combination of the two channels.

Preliminary Results for Winter 2006 Conferences

In the standard model (SM) the Higgs boson is crucial to the understanding of electroweak symmetry breaking and the mass generation of electroweak gauge bosons and fermions. Direct searches at the CERN e^+e^- collider (LEP) yield a lower limit for the Higgs boson mass of $m_H > 114.4$ GeV [1] at 95% CL. Indirect measurements via fits to the electroweak precision data give an upper bound of $m_H < 251$ GeV [2] at 95% confidence limit.

In this note a search for Higgs bosons decaying to the WW^* final state in the $D\bar{O}$ experiment at the Tevatron is presented. To achieve a good signal-to-background ratio, the leptonic decay modes $H \rightarrow WW^* \rightarrow ll'$ ($l, l' = e, \mu$) are considered, leading to final states with two leptons and missing transverse momentum. This decay mode provides the largest sensitivity for the Standard Model Higgs boson search at the Tevatron at a mass of $M_H \sim 160$ GeV [3–5]. If combined with searches exploiting the WH and ZH associated production, this decay mode increases the sensitivity for the Higgs boson searches in the low mass region $M_H \sim 120$ GeV.

Upper limits on the $H \rightarrow WW^* \rightarrow ll'$ ($l, l' = e, \mu$) cross section with smaller data sets have already been presented in Ref. [6]. In the present analysis the larger $D\bar{O}$ dataset available is included; however, so far only e^+e^- and $e^\pm\mu^\mp$ final states have been considered. Upper limits on the production cross section times branching ratio $\sigma \times BR(H \rightarrow WW^*)$ are presented using the combination of these two channels. The data sample used in this analysis has been collected between April 2002 and November 2005 by the $D\bar{O}$ detector at the Fermilab Tevatron collider at $\sqrt{s} = 1.96$ TeV, corresponding to a luminosity of the order of 950 pb^{-1} in both the e^+e^- and $e^\pm\mu^\mp$ final states.

We briefly describe the main components of the $D\bar{O}$ Run II detector [7] important to this analysis. The central tracking system consists of a silicon microstrip tracker (SMT) and a central fiber tracker (CFT), both located within a 2.0 T axial magnetic field. The SMT strips have a typical pitch of 50–80 μm , and the design is optimized for tracking and vertexing over the pseudorapidity range $|\eta| < 3$, where $\eta = -\ln(\tan \frac{\theta}{2})$ with polar angle θ . The system has a six-barrel longitudinal structure, with each barrel a set of four silicon layers arranged axially around the beam pipe, interspersed with sixteen radial disks. The CFT has eight thin coaxial barrels, each supporting two doublets of overlapping scintillating fibers of 0.835 mm diameter, one doublet parallel to the beam axis, the other alternating by $\pm 3^\circ$ relative to the beam axis.

A liquid-argon/uranium calorimeter surrounds the central tracking system and consists of a central calorimeter (CC) covering to $|\eta| \approx 1.1$, and two end calorimeters (EC) extending coverage for $|\eta| < 4.2$, each housed in separate cryostats [8]. Scintillators between the CC and EC cryostats provide sampling of showers for $1.1 < |\eta| < 1.4$.

The muon system is located outside the calorimeters and consists of a layer of tracking detectors and scintillation trigger counters inside toroid magnets which provide a 1.8 T magnetic field, followed by two similar layers behind each toroid. Tracking in the muon system for $|\eta| < 1$ relies on 10 cm wide drift tubes [8], while 1 cm mini-drift tubes are used for $1 < |\eta| < 2$ [9].

The $H \rightarrow WW^* \rightarrow ll'$ ($l, l' = e, \mu$) candidates are selected by triggering on single or di-lepton events using a three level trigger system. The first trigger level uses hardware to select electron candidates based on energy deposition in the electromagnetic part of the calorimeter and selects muon candidates formed by hits in two layers of the muon scintillator system. Digital signal processors in the second trigger level form muon track candidate segments defined by hits in the muon drift chambers and scintillators. At the third level, software algorithms running on a computing farm and exploiting the full event information are used to make the final selection of events which are recorded for offline analysis.

In the further offline analysis electrons are identified by electromagnetic showers in the calorimeter. These showers are chosen by comparing the longitudinal and transverse shower profiles to those of simulated electrons. The showers must be isolated, deposit most of their energy in the electromagnetic part of the calorimeter, and pass a likelihood criterion that includes a spatial track match and, in the CC region, an E/p requirement, where E is the energy of the calorimeter cluster and p is the momentum of the track. All electrons are required to be in the pseudorapidity range $|\eta| < 3.0$. The transverse momentum measurement of the electrons is based on calorimeter cell energy information.

Muon tracks are reconstructed from hits in the wire chambers and scintillators in the muon system and must match a track in the central tracker. To select isolated muons, the scalar sum of the transverse momentum of all tracks other than that of the muon in a cone of $\mathcal{R} = 0.5$ around the muon track must be less than 4 GeV, where $\mathcal{R} = \sqrt{(\Delta\phi)^2 + (\Delta\eta)^2}$ and ϕ is the azimuthal angle. Muon detection is restricted to the coverage of the muon system $|\eta| < 2.0$. Muons from cosmic rays are rejected by requiring a timing criterion on the hits in the scintillator layers as well as applying restrictions on the position of the muon track with respect to the primary vertex.

The decay of two W bosons into electrons or muons results in three different final states $e^+e^- + X$ (ee channel), $e^\pm\mu^\mp + X$ ($e\mu$ channel), and $\mu^+\mu^- + X$ ($\mu\mu$ channel), each of which consists of two oppositely charged isolated high transverse momentum, p_T , leptons and large missing transverse energy, \cancel{E}_T , due to the escaping neutrinos. The event kinematics change significantly as a function of Higgs mass. The analysis sensitivity is improved by using selection requirements which depend on the Higgs mass, thereby reflecting the changing kinematics [3]. The list of the mass dependent cuts used in the current analysis is in Table I. Four Higgs masses M_H from 120 GeV to 180 GeV have been chosen.

In both e^+e^- and $e^\pm\mu^\mp$ final states, two leptons originating from the same vertex are required to be of opposite

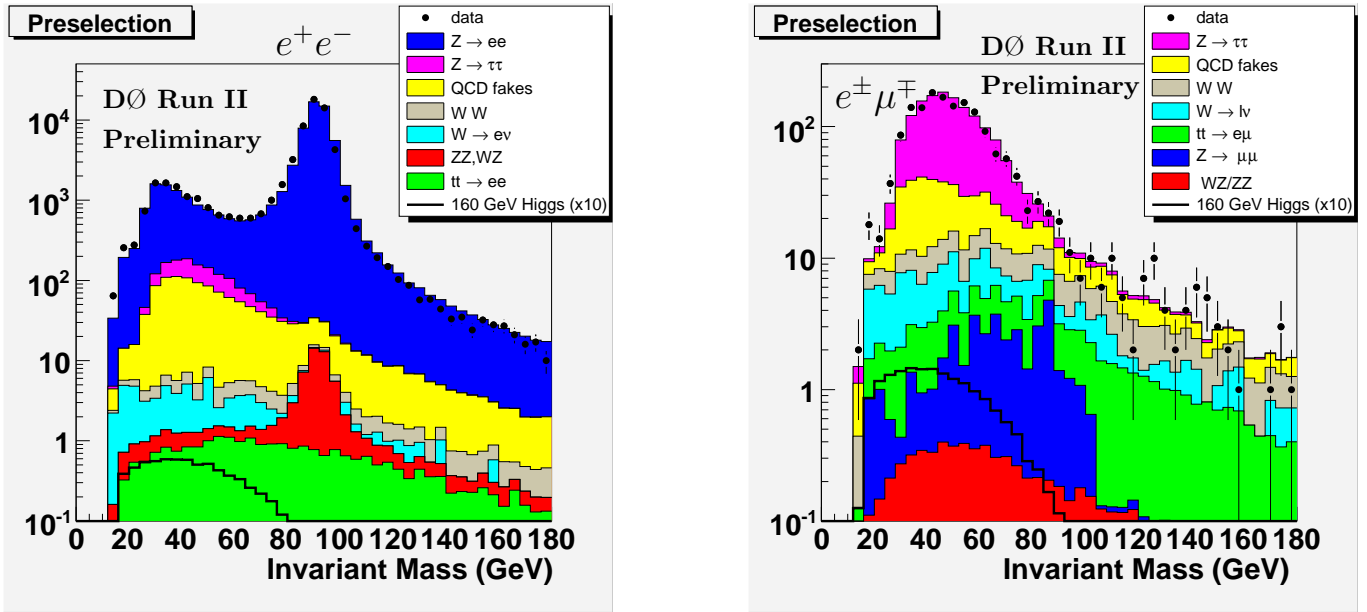


FIG. 1: Distribution of the invariant mass $M_{ll'}$ after the initial transverse momentum and di-lepton invariant mass cuts (Cut 1, preselection) for the e^+e^- (left) and $e^\pm\mu^\mp$ (right) final states. The expected signal, multiplied by a factor of 10, for the Standard Model Higgs of mass 160 GeV is also shown.

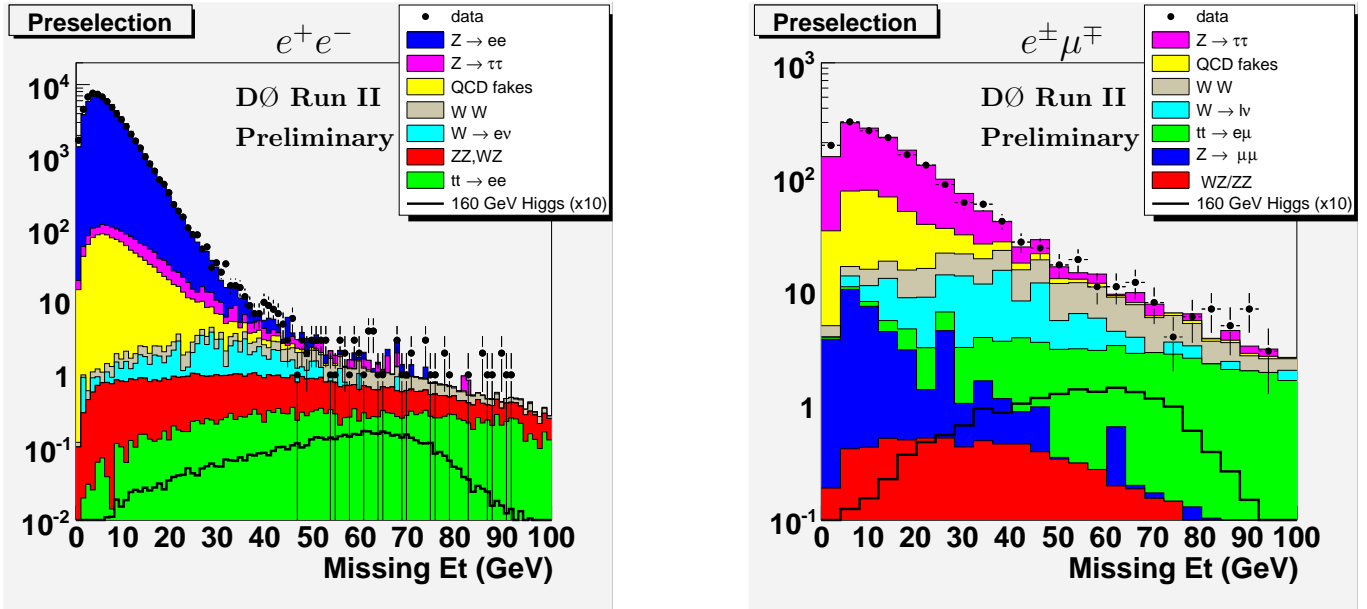


FIG. 2: Distribution of the missing transverse energy \cancel{E}_T after the initial transverse momentum and di-lepton invariant mass cuts (Cut 1, preselection) for the e^+e^- (left) and $e^\pm\mu^\mp$ (right) final states. The expected signal, multiplied by a factor of 10, for the Standard Model Higgs of mass 160 GeV is also shown.

charge, and must have $p_T^e > 15$ GeV for the leading electron and $p_T^e > 10$ GeV for the trailing one in the e^+e^- channel, and $p_T^e > 15$ GeV for the electron and $p_T^\mu > 10$ GeV for the muon in the $e^\pm\mu^\mp$ final state. In addition, the di-lepton invariant mass is required to exceed 15 GeV (Cut 1, preselection). In Figs. 1 and 2, the comparison between data and Monte Carlo (MC) is shown for the invariant mass of the dilepton system and the missing transverse energy at the preselection level. Figure 3 shows the good agreement between data and MC in $\Delta\phi_{ll'}$ distributions for the e^+e^- channel (a) and the $e^\pm\mu^\mp$ channel (c) after applying the lepton transverse momentum and di-lepton invariant mass cuts. In both channels, the background is largely dominated by Z/γ^* production which is suppressed by requiring the missing transverse energy \cancel{E}_T to be greater than 20 GeV (Cut 2). Events are further removed if the \cancel{E}_T could

Selection criterion	Value
Cut 1 Preselection	Trigger, ID, leptons with opposite charge and $p_T^l > 15$ GeV and $p_T^{\nu} > 10$ GeV, $m_{ll} > 15$ GeV ($H \rightarrow WW^* \rightarrow e\mu$: remove events with 2e or 2 μ , if $75 \text{ GeV} < M_{ll} < 105 \text{ GeV}$)
Cut 2 Missing transverse energy \cancel{E}_T	$\cancel{E}_T > 20 \text{ GeV}$
Cut 3 $\cancel{E}_T^{\text{Scaled}}$	$\cancel{E}_T^{\text{Scaled}} > 7$ (for $N_{Jet} > 0$)
Cut 4 Invariant mass $M_{ll'}$	$M_{ee} < \min(M_H/2, 80) \text{ GeV}$ $M_{e\mu} < M_H/2 \text{ GeV}$
Cut 5 Sum of $p_T^l + p_T^{\nu} + \cancel{E}_T$	$M_H/2 + 20 \text{ GeV} < p_T^l + p_T^{\nu} + \cancel{E}_T < M_H$
Cut 6 $M_{min}^T(l, \cancel{E}_T)$	$M_{min}^T(l, \cancel{E}_T) > 45 \text{ GeV} (M_H = 120 \text{ GeV})$ $M_{min}^T(l, \cancel{E}_T) > 50 \text{ GeV} (M_H = 140 \text{ GeV})$ $M_{min}^T(l, \cancel{E}_T) > 55 \text{ GeV} (M_H = 160 \text{ GeV})$ $M_{min}^T(l, \cancel{E}_T) > 60 \text{ GeV} (M_H = 180 \text{ GeV})$
Cut 7 H_T (scalar sum of p_T^{jet})	$H_T < 100 \text{ GeV}$
Cut 8 Lepton opening angle $\Delta\phi_{ll'}$	$\Delta\phi_{ll'} < 2.0$

TABLE I: Summary of the selection criteria for a Higgs mass M_H dependent selection.

have been produced by a mis-measurement of jet energies. The fluctuation in the measurement of jet energy in the transverse plane can be approximated by $\Delta E^{\text{jet}} \cdot \sin \theta^{\text{jet}}$ where ΔE^{jet} is proportional to $\sqrt{E^{\text{jet}}}$. The opening angle $\Delta\phi(\text{jet}, \cancel{E}_T)$ between this projected energy fluctuation and the missing transverse energy provides a measure of the contribution of the jet to the missing transverse energy. The scaled missing transverse energy defined as:

$$\cancel{E}_T^{\text{Scaled}} = \frac{\cancel{E}_T}{\sqrt{\sum_{\text{jets}} (\Delta E^{\text{jet}} \cdot \sin \theta^{\text{jet}} \cdot \cos \Delta\phi(\text{jet}, \cancel{E}_T))^2}} \quad (1)$$

is required to be greater than 7 (Cut 3). The cuts on the invariant mass of the dilepton system (Cut 4), the sum of the lepton transverse momenta and the missing transverse energy (Cut 5) and on the minimal transverse mass between the lepton and the missing transverse energy (Cut 6) are Higgs mass dependent and optimized to further suppress contributions from $Z/\gamma^*, WW, WZ, ZZ, W \rightarrow l\nu$ backgrounds. Since the charged lepton system and the two neutrinos are emitted back-to-back, the invariant mass for the Higgs decays is restricted to $M_H/2$. Thus, depending on the Higgs mass M_H the invariant mass $M_{ll'}$ is required to be $M_{ll'} < M_H/2 \text{ GeV}$ (Cut 4). The sum of the lepton transverse momentum p_T and the missing transverse momentum \cancel{E}_T is required to be in the range $M_H/2 + 20 \text{ GeV} < p_T^l + p_T^{\nu} + \cancel{E}_T < M_H$ (Cut 5). The minimal transverse energy $M_{min}^T(l, \cancel{E}_T)$ (l,MET) between lepton and \cancel{E}_T (Cut 6) in the event $M_T(l, \cancel{E}_T) = \sqrt{2p_T^l \cancel{E}_T (1 - \cos \Delta\phi(l, \cancel{E}_T))}$ is required to be more than 45,50,55,60 GeV for the Higgs masses 120,140,160 and 180 GeV, respectively. $t\bar{t}$ events are further rejected by a cut on $H_T < 100$ GeV, the scalar sum of the p_T of good jets in the event (Cut 7). Finally, the spin correlations in the decay of the Higgs boson are used. The leptons of the Higgs decay tend to have a small opening angle, whereas leptons from most of the backgrounds are expected to be back-to-back. Thus it is required that the opening angle between the leptons in the transverse plane $\Delta\phi_{ll'}$ is smaller than 2.0. Fig. 3 presents the distributions of the lepton opening angle in the transverse plane $\Delta\phi_{ll'}$ after the final selection (Cuts 1-7), except for the $\Delta\phi_{ll'}$ criterion, for the b) e^+e^- and d) $e^\pm\mu^\mp$ final states.

The signal and Standard Model background processes have been generated with PYTHIA 6.319 [10] using the CTEQ6.1M parton distribution functions, followed by a detailed GEANT-based [11] simulation of the DØ detector. The overall detection efficiency ranges from $(7.2 \pm 0.2)\%$ to $(17.7 \pm 0.2)\%$ depending on the decay channel and the M_H dependent selection. Table II summarizes all these numbers. Using the NLO cross sections calculated with HDECAY [12] and HIGLU [13] and branching fractions BR of 0.1072 ± 0.0016 for $W \rightarrow e\nu$ and 0.1057 ± 0.0022 for $W \rightarrow \mu\nu$ [14], the expected number of events for $H \rightarrow WW^* \rightarrow l^+l^- (ee, e\mu)$ is $1.38 \pm 0.01(\text{stat})$ events for a Higgs boson mass $M_H = 160 \text{ GeV}$. The expected signal for all four Higgs masses is given by the first line of Table III.

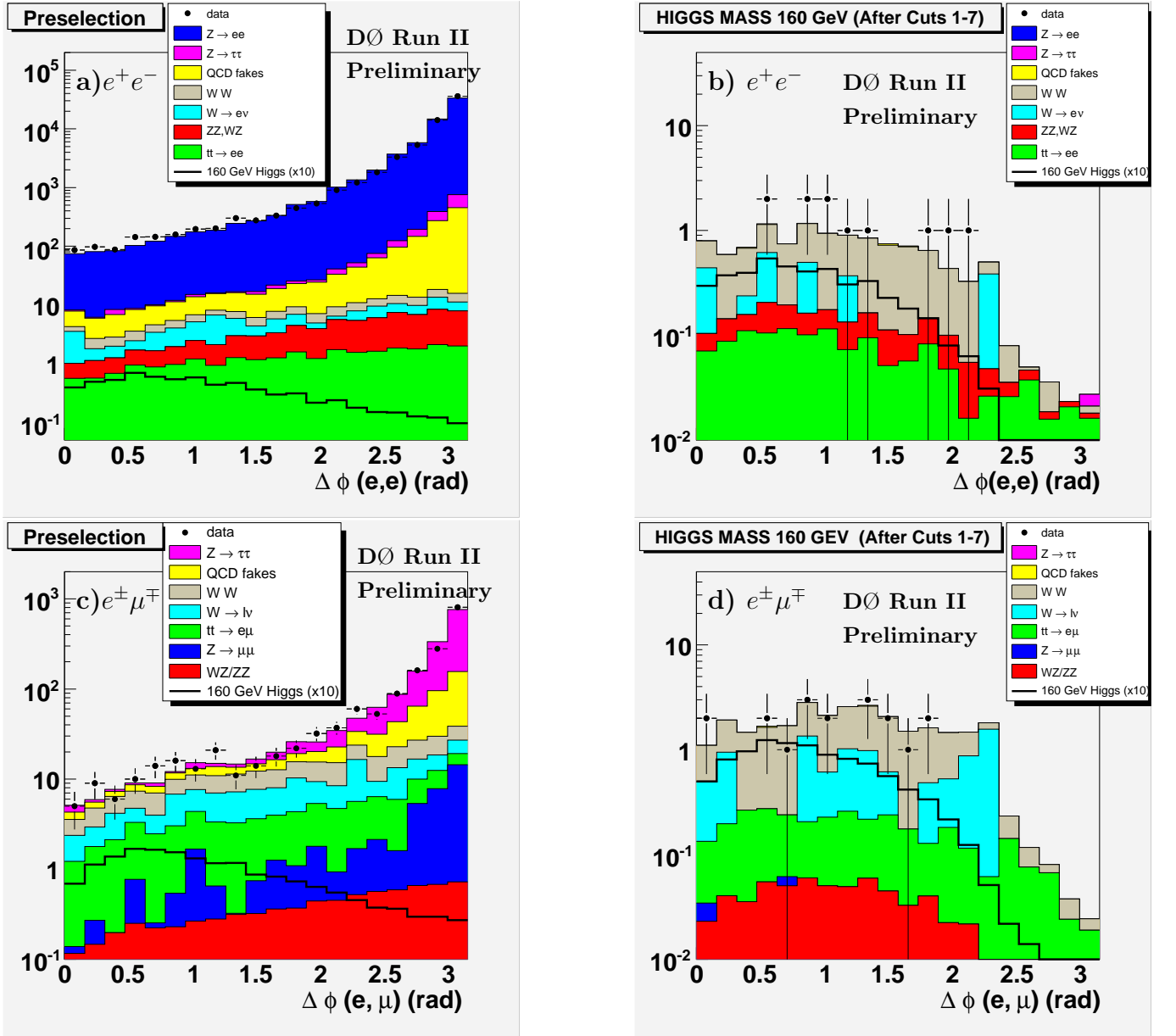


FIG. 3: Distribution of the opening angle $\Delta\phi_{ll}$ after applying the initial transverse momentum and di-lepton invariant mass cuts in the (a) e^+e^- , (c) $e^\pm\mu^\mp$ channel. Figures (b), (d) show the $\Delta\phi_{ll}$ distributions after the final selection (Cuts 1-7), except for the $\Delta\phi_{ll}$ criterion, for the e^+e^- and $e^\pm\mu^\mp$ final states, respectively. The expected signal, multiplied by a factor of 10, for the Standard Model Higgs of mass 160 GeV is also shown.

The $Z/\gamma \rightarrow ll$ cross section is calculated with CTEQ6.1M PDFs as $\sigma(Z/\gamma \rightarrow ll) = \sigma_{LO} \times K_{QCD}(Q^2)$, with the LO cross section calculated by Pythia LO PDF and the K_{QCD} at NNLO with NLO PDF, calculated according to [15, 16]. The cross section times branching ratio of $Z/\gamma \rightarrow ll$ production in the invariant mass region $60 \text{ GeV} < M_{ll} < 130 \text{ GeV}$ is $\sigma \times BR = 241.6 \text{ pb}$. The $W \rightarrow e\nu$ background level is calculated with NNLO corrections and CTEQ6.1M as listed in [16]. For inclusive W boson production with decays into a single lepton flavor state this value is $\sigma \times BR = 2583 \text{ pb}$. The calculations of Ref. [17] are used for $t\bar{t}$ production with $\sigma \times BR = 0.076 \text{ pb}$ with single flavor lepton decays of both W bosons. The NLO WW , WZ and ZZ production cross section values are taken from Ref. [18] with $\sigma \times B = 0.15 \text{ pb}$ for WW , $\sigma \times B = 0.014 \text{ pb}$ for WZ and $\sigma \times B = 0.002 \text{ pb}$ for ZZ production with decay into a single lepton flavor state. The background due to multijet production, when a jet is misidentified as an electron, is determined from the data using a sample of like-sign di-lepton events with inverted lepton quality cuts (called QCD fakes in Figs. 3).

For the e^+e^- final state, the normalization used in this analysis is a factor that scales the NNLO $Z/\gamma^* \rightarrow ee$ cross

TABLE II: Efficiencies (%) with statistical errors for $H \rightarrow WW^* \rightarrow e^+e^-$ or $e^\pm\mu^\mp$ decays after all cuts.

M_H (GeV)	e^+e^-	$e^\pm\mu^\mp$
120	7.2 ± 0.2	7.4 ± 0.2
140	10.7 ± 0.2	12.7 ± 0.2
160	15.9 ± 0.2	17.7 ± 0.2
180	14.7 ± 0.2	17.7 ± 0.2

TABLE III: Number of signal and background events expected and number of events observed after all selections are applied for the combination of e^+e^- and $e^\pm\mu^\mp$ channels. Only statistical uncertainties are given.

M_H (GeV)	120	140	160	180
$H \rightarrow WW$	0.2 ± 0.01	0.75 ± 0.01	1.38 ± 0.01	0.90 ± 0.01
$Z/\gamma \rightarrow ll$	0.8 ± 0.6	0.4 ± 0.4	0.02 ± 0.01	0.02 ± 0.01
Diboson (WW, WZ)	16.4 ± 0.2	22.3 ± 0.2	24.6 ± 0.2	22.3 ± 0.2
$t\bar{t}$	0.8 ± 0.1	1.9 ± 0.1	3.2 ± 0.1	4.1 ± 0.1
$W + jet/\gamma$	14.4 ± 2.1	11.4 ± 2.0	6.7 ± 1.6	4.5 ± 1.3
Multijet	0.4 ± 0.4	0.3 ± 0.3	0.2 ± 0.2	0.2 ± 0.2
Background sum	32.7 ± 2.3	36.2 ± 2.1	34.7 ± 1.7	31 ± 1.4
Data	31	35	28	23

section (see Fig. 1) to the data in the mass region $60 \text{ GeV} < M_{ee} < 130 \text{ GeV}$. For the $e^\pm\mu^\mp$ final state, the data sample size is determined by normalizing the electron-muon invariant mass distribution (see Fig. 1) to the NNLO $Z/\gamma^* \rightarrow \tau\tau$ cross section. The estimated data sample size both for the di-electron and electron-muon final states was found to be of the order of $\sim 950 \text{ pb}^{-1}$. Data/MC electron correction factors have been applied to MC before normalization to $Z/\gamma^* \rightarrow ee$. No data/MC muon correction factors (trigger turn-on, muon and track reconstruction efficiencies) have been applied and they are absorbed in the normalization to $Z/\gamma^* \rightarrow \tau\tau$. By using this method to estimate data sample size, the limit on the $H \rightarrow WW^* \rightarrow ll'$ ($l, l' = e, \mu$) cross section is calculated relative to the NNLO $Z/\gamma^* \rightarrow ll$ cross section. Systematic errors, coming from the luminosity determination, on data/MC correction factors are canceled by using such a normalization procedure.

A summary of the background contributions together with signal expectations and events observed in the data after the final selection is shown in Table III. Since after all selection cuts the remaining candidate events are consistent with the background expectation, limits on the production cross section times branching ratio $\sigma \times BR(H \rightarrow WW^*)$ are derived using a method described in Ref. [19]. This method calculates the cross section limits at 95% C.L. with the integrated luminosity, number of background events, signal acceptance and number of events in data with corresponding errors as inputs. The uncertainty on the background was determined from the statistical and systematic uncertainty.

Various sources of systematic uncertainties affect the background estimation and the signal efficiency of $H \rightarrow WW^*$ production in e^+e^- and $e^\pm\mu^\mp$ final states: theoretical uncertainty of WW, $t\bar{t}$ and Z/γ^* production cross sections, Jet Energy Scale (JES), electron and muon reconstruction efficiencies and resolutions. In the low mass region, the uncertainty is dominated by the jet energy scale and variations in the $W + jet/\gamma$ contribution. With increasing Higgs mass, this uncertainty is decreasing because of the decreasing contribution of $W + jet/\gamma$ events. Since the WW production is the dominant background for Higgs bosons above $M_H = 160 \text{ GeV}$, the systematic uncertainty is dominated by the error on the WW production cross section. Until the systematic errors are completely studied, conservative systematic errors of 10 % and 15 % for the signal and background respectively, based on the previous results [6], are used. The systematic error on the normalization factor is conservatively taken to be 5 %. It results from the NNLO $Z/\gamma^* \rightarrow ll$ cross section uncertainty (3.6 %) and statistical error on data/MC normalization factor ~ 1 % for the e^+e^- and ~ 3 % for the $e^\pm\mu^\mp$ channel.

Table IV presents observed upper limits at 95% C.L on the cross section times branching ratio for the combination of e^+e^- and $e^\pm\mu^\mp$ final states for four different Higgs boson masses M_H . The combination of e^+e^- and $e^\pm\mu^\mp$ channels was performed by multiplying the individual likelihood functions of these channels resulting into a combined likelihood function. Fig. 4 shows the calculated expected and observed cross section limits for $\sigma \times BR(H \rightarrow WW^*)$ for the different Higgs boson masses compared with predictions from the SM and from similar models with 4 fermion families [20, 21]. With the current dataset no region of the SM prediction can be excluded.

A search for the Higgs boson is presented in $H \rightarrow WW^* \rightarrow ll'$ ($l, l' = e, \mu$) decays in $p\bar{p}$ collisions at a center-of-mass energy of $\sqrt{s} = 1.96 \text{ TeV}$. The data, collected from April 2002 to November 2005 with the Run II DØ detector, correspond to an integrated luminosity of the order of $\sim 950 \text{ pb}^{-1}$ in the e^+e^- and $e^\pm\mu^\mp$ final states. The number of

TABLE IV: Observed upper limits at 95% C.L. on the cross section times branching ratio for $\sigma \times BR(H \rightarrow WW^*)$ for the combination of e^+e^- and $e^\pm\mu^\mp$ final states for different Higgs boson masses M_H .

M_H (GeV)	120	140	160	180
Upper Limits (pb)	6.3	4.1	2.2	1.9

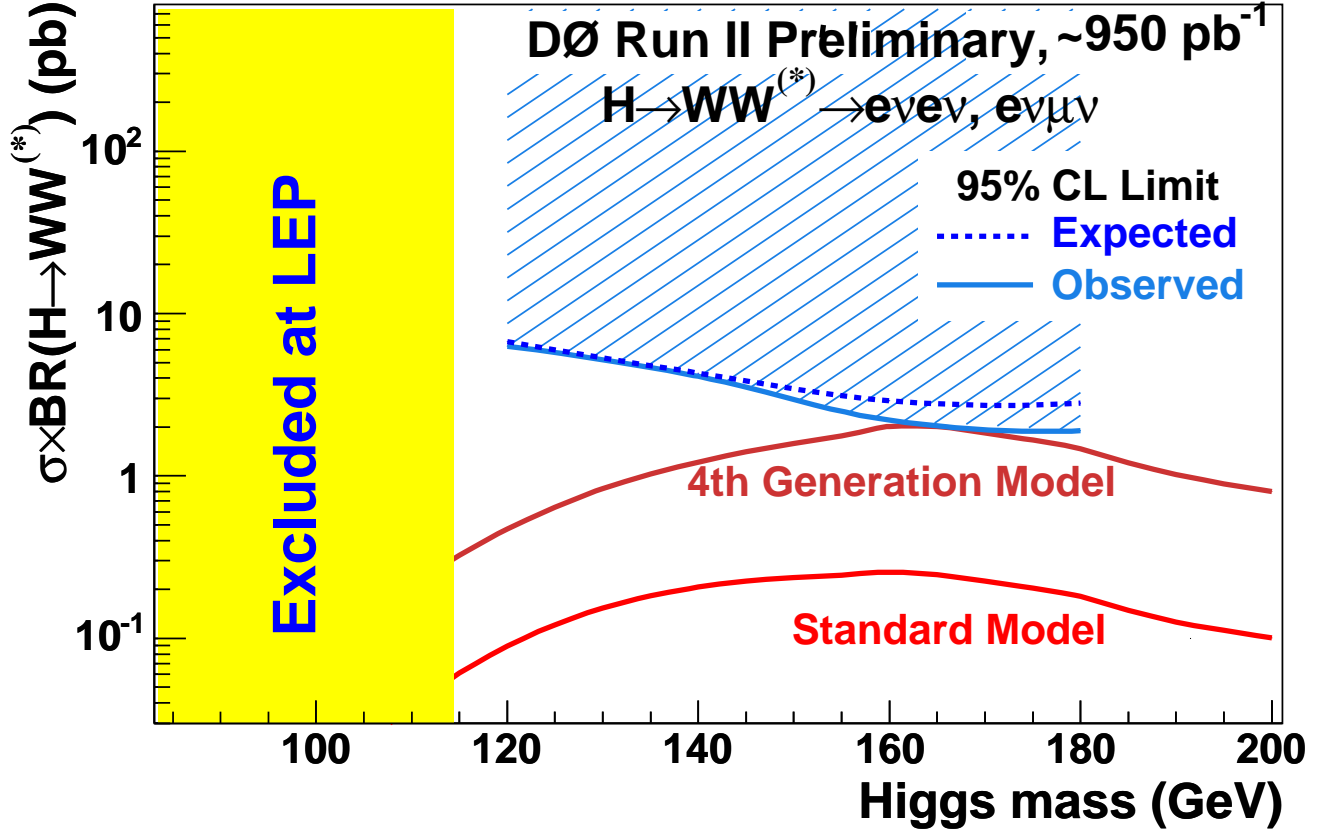


FIG. 4: Excluded cross section times branching ratio $\sigma \times BR(H \rightarrow WW^*)$ at 95% CL together with expectations from standard model Higgs boson production and alternative models derived using a Modified Frequentist Approach. The LEP limit on the standard model Higgs boson production is taken from [1] and the 4th generation model is discussed in [20, 21].

events observed is consistent with expectations from standard model backgrounds. Limits for the combination of two channels on the production cross section times branching ratio $\sigma \times BR(H \rightarrow WW^*)$ are presented.

-
- [1] R. Barate *et al.*, Phys. Lett. B **565** (2003) 61.
[2] The LEP Collaborations, the LEP Electroweak Group, the SLD Electroweak and Heavy Flavours Group, “A combination of preliminary electroweak measurements and constraints on the standard model,” arXiv:hep-ex/0412015.
[3] T. Han, A. Turcot, R-J. Zhang, Phys. Rev. D. **59**, 093001 (1999).
[4] M. Carena *et al.* [Higgs Working Group Collaboration], “Report of the Tevatron Higgs working group”, hep-ph/0010338.
[5] K. Jakobs, W. Walkowiak, ATLAS Physics Note, ATL-PHYS-2000-019.
[6] J. Elmsheuser, M. Hohlfeld, DØ Note 4759; Phys. Rev. Lett. **96**, 011801 (2006)
[7] DØ Collaboration, V. Abazov *et al.*, to be published in Nucl. Instrum. Methods A; arXiv:physics/0507191.
[8] DØ Collaboration, S. Abachi *et al.*, Nucl. Instrum. Methods Phys. Res. A **338**, 185 (1994).
[9] V. Abramov *et al.*, Nucl. Instrum. Meth. A **419**, 660 (1998).
[10] T. Sjöstrand *et al.*, Comp. Phys. Comm. **135**, 238 (2001).

- [11] R. Brun and F. Carminati, CERN Program Library Long Writeup W5013, 1993 (unpublished).
- [12] A. Djouadi et al., Comput. Phys. Commun. **108**, 56 (1998).
- [13] M. Spira, Report DESY T-95-05 (October 1995), arXiv:hep-ph/9510347.
- [14] Particle Data Group, S. Eidelman *et al.*, Phys. Lett. B **592**, 1 (2004).
- [15] R. Hamberg, W.L. van Neerven, and T. Matsuura, Nucl. Phys. **B359**, 343 (1991) [Erratum-ibid. **B644**, 403 (2002)].
- [16] T. Nunnemann, DØ Note 4476.
- [17] N. Kidonakis and R. Vogt, Phys. Rev. D **68**, 114014 (2003).
- [18] J. M. Campbell and R. K. Ellis, Phys. Rev. D **60**, 113006 (1999).
- [19] T. Junk, Nucl. Instr. and Meth., A434(1999) 435.
- [20] E. Arik, O. Cakir, S.A Cetin and S. Sultansoy, arXiv:hep-ph/0502050.
- [21] E. Arik, M. Arik, S. A. Cetin, T. Conka, A. Mailov and S. Sultansoy, Eur. Phys. J. C **26**, 9 (2002).